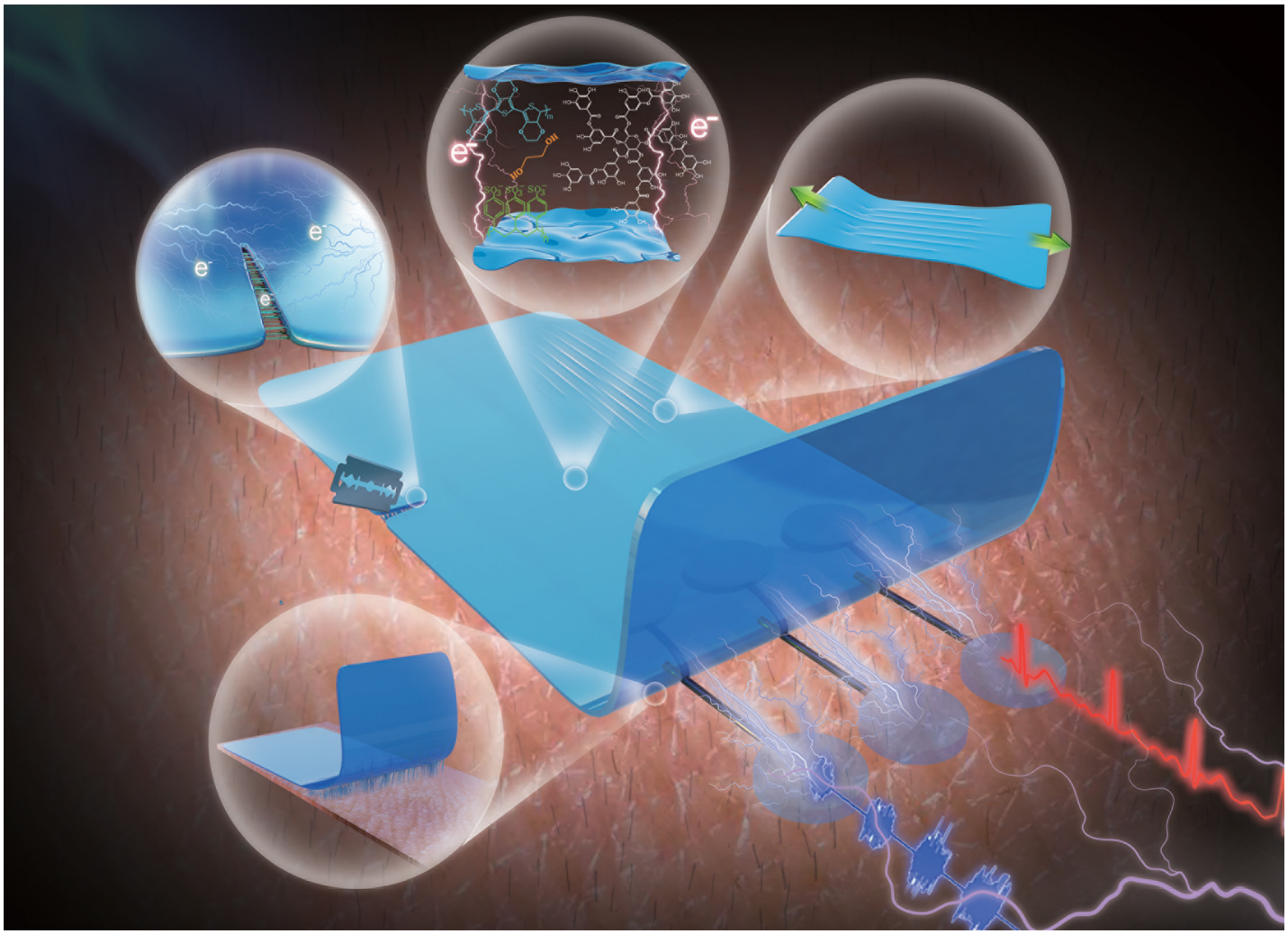

Showing research from the Department of Chemical Engineering, Polytechnique Montréal, Montréal, Canada.

Conducting polymer films and bioelectrodes combining high adhesion and electro-mechanical self-healing

Soft films obtained from PEDOT:PSS, ethylene glycol, and tannic acid exhibited a low Young's modulus of ~450 kPa, high adhesion on the skin, stretchability of ~90% strain, outstanding self-healing ability, and biocompatibility. Epidermal electrodes prepared using the films demonstrated high-quality electrocardiography and electromyography signal recordings.

As featured in:

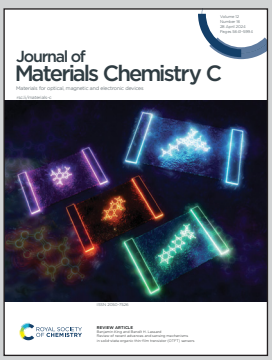

See Fabio Cicoira *et al.*, *J. Mater. Chem. C*, 2024, **12**, 5708.

ROYAL SOCIETY OF CHEMISTRY

rsc.li/materials-c

Registered charity number: 207890

Journal of Materials Chemistry C

ROYAL SOCIETY OF CHEMISTRY

PAPER

View Article Online
View Journal | View Issue

Cite this: J. Mater. Chem. C, 2024, 12, 5708

Conducting polymer films and bioelectrodes combining high adhesion and electro-mechanical self-healing†

Xin Zhou, [a] Pierre Kateb, [a] Jiaxin Fan, [a] Jinsil Kim, [a] Gregory A. Lodygensky, [b] Bénédicte Amilhon, [bc] Damiano Pasini [d] and Fabio Cicoira *[a]

Received 16th November 2023,
Accepted 12th December 2023

DOI: 10.1039/d3tc04230h

rsc.li/materials-c

Self-healable, conductive, soft, and stretchable electronic materials have become research hotspots in wearable and bioelectronic devices for healthcare monitoring. In this study, conductive, soft, stretchable, self-healing, highly adhesive, and biocompatible conductive polymer films were obtained by mixing poly(3,4-ethylenedioxythiophene) doped with polystyrene sulfonate (PEDOT:PSS), ethylene glycol (EG), and tannic acid (TA). The films with optimized composition demonstrated very attractive properties for wearable electronics and bioelectronics, including a conductivity of ~17 S cm^{-1}, a low Young's modulus of ~450 kPa, stretchability of ~90% strain, outstanding electrical stability during stretching (2% resistance change at 30% strain), and strong adhesion on several substrates. Notably, the films exhibited outstanding autonomous and cut-stick healing properties, enabled by the addition of TA. Furthermore, the films exhibited no signs of cytotoxicity, making them suitable for biomedical applications. Epidermal electrodes prepared using these materials exhibit low skin-electrode impedance at low frequencies (1–100 Hz) and high quality for electrocardiography (ECG) and electromyography (EMG) signal recordings. This study promotes the development of innovative wearable biomedical devices and contribute to personalized healthcare monitoring.

1. Introduction

Materials encompassing electrical conductivity, softness, stretchability, adhesion, and self-healing properties are in high demand for applications in bioelectronics, wearable electronics, and energy storage.[1–9] In particular, epidermal bioelectronic devices require a delicate balance between mechanical and electrical properties, *i.e.*, (i) low Young's modulus (*e.g.*, 60–850 kPa for skin and muscles), to reduce the mismatch between the electrodes and bio-tissues that could lead to signal deterioration and skin damage; (ii) high adhesion and conformal contact on the skin; (iii) reasonable electrical conductivity; and (iv) ability to retain mechanical and electrical performance over time.[10,11] Materials with such characteristics can be obtained by mixing organic conducting polymers, which typically exhibit modest mechanical properties, with other polymers capable of imparting desired mechanical functionalities.[1,11]

The conducting polymer poly(3,4-ethylenedioxythiophene) doped with polystyrene sulfonate (PEDOT:PSS), in the form of an aqueous suspension, can be mixed with a wide range of water-soluble molecular, polymeric, and ionic materials. Flexible and stretchable conductors have been obtained by mixing this material with polyols (*e.g.*, xylitol, glycerol, and ethylene glycol (EG)), ionic liquids, and polymers, such as polyvinyl alcohol (PVA), poly(ethylene oxide) (PEO), polyethylene glycol (PEG), and Triton X-100. In addition, several materials based on PEDOT:PSS exhibit self-healing properties, which greatly benefit the performance and sustainability of epidermal electronics.[10,12–14] Last but not least, mixing also allows to control the adhesion strength of PEDOT:PSS based materials, which is critical for epidermal electronics. Adhesive films made from a blend of PEDOT:PSS, waterborne polyurethane (WPU), and D-sorbitol,[15] exhibited a Young's modulus of ~40 MPa, good adhesion on dry skin (~0.4 N cm^{-1}) and could achieve high quality bio-potential recording. Soft adhesive films prepared from a mixture of β-cyclodextrin, citric acid, PVA, glutaraldehyde, and PEDOT:PSS exhibited a low modulus of ~400 kPa, high stretchability

[a] Department of Chemical Engineering, Polytechnique Montréal, Montréal, QC H3C 3A7, Canada. E-mail: fabio.cicoira@polymtl.ca
[b] CHU Sainte-Justine Hospital Research Center, Montréal, QC H3T 1C5, Canada
[c] Department of Neurosciences, University of Montréal, Montréal, QC H3T 1J4, Canada
[d] Department of Mechanical Engineering, McGill University, Montréal, QC H3A 0C3, Canada

† Electronic supplementary information (ESI) available. See DOI: https://doi.org/10.1039/d3tc04230h

(~700 strain), high interface adhesion (~1.2 MPa on a polyimide substrate), and a conductivity of ~37 S cm^{-1}. These films have been used as epidermal electrodes for electromyographic signal monitoring.[1] Tannic acid (TA), a natural polyphenol, is widely used to improve the adhesion strength of PEDOT-based materials on several substrates, including human skin.[16,17] Adhesive films obtained from PEDOT:PSS, PVA, EG, and TA exhibited a stretchability approximately up to 50% strain, a Young's modulus of ~18 MPa, and good adhesion to porcine skin (~0.3 N cm^{-1}).[18] TA has also been used to prepare self-healing hydrogels in combination with poly(dimethyldiallylammonium chloride) (PDDA)) and FeIII,[19] thioctic acid,[20] silk fibroin,[21] and PVA/PAAM.[22] Besides its effect on the mechanical properties, TA offers biocompatibility as well as antibacterial, antioxidative, and anti-inflammatory properties.[16,17,23] Moreover, TA has been shown to increase the conductivity of PEDOT:PSS films.[24]

Significant progresses have been achieved on the mechanical and electrical properties and bio-signal recording performance of epidermal electrodes. Cao *et al.* developed stretchable and self-adhesive dry electrodes based on PEDOT:PSS/EG/PVA/TA, the film exhibited a high conductivity of 120 S cm^{-1}, moderate stretchability, and ~15% resistance change at 30% strain.[18] Another PEDOT:PSS based composite composed of citric acid, cyclodextrin, PVA, which were covalently crosslinked by glutaraldehyde, was shown to be highly stretchable (700%) with moderate conductivity.[1] The film developed based on PEDOT:PSS, waterborne polyurethane, and D-sorbitol exhibited a very high electrical conductivity ~545 S cm^{-1} with moderate stretchability.[15] The PEDOT:PSS, glycerol, and polysorbate films demonstrated satisfactory mechanical and electrical properties with limited adhesiveness.[25] However, despite these remarkable advancements, the self-healing properties of epidermal electronic materials have received limited attention.

In this study, we reported a conductive material obtained from an aqueous mixture of PEDOT:PSS, EG, and TA. The main novelty of this material is the combination of high adhesion, biocompatibility, highly electrical stability, and electro-mechanical self-healing properties. Films obtained from this material exhibited a low Young's modulus (~450 kPa), electrical conductivity of ~17 S cm^{-1}, high stretchability, high interfacial adhesion on glass and porcine skin, and outstanding electrical and mechanical self-healing properties. Cell viability assays showed no evidence of cell toxicity. Soft epidermal film electrodes based on these materials showed performance comparable to that of commercial Ag/AgCl gel electrodes for ECG and EMG recordings. The ease of processing, environmental sustainability, biocompatibility, and well-balanced electromechanical properties of this material make it ideal for applications in bioelectronics and wearable electronics.

2. Experimental section

2.1 Materials

Tannic acid (TA), ethylene glycol (EG), and isopropyl alcohol (IPA) were obtained from Millipore Sigma (St. Louis, Mo, USA). PEDOT:PSS (Clevios™ PH1000 aqueous suspension) was purchased from Heraeus Precious Metals (Germany). The PEDOT:PSS content in this formulation declared by the supplier was between 1 and 1.3%. Silver ink (Ag 520 EI) was donated by Chimet Sp.A (Italy). PET sheets (XF-122, 25 μm thick) were purchased from Polyonics (USA). Glass slides were obtained from Corning (USA). Porcine skin samples were obtained from a local grocery store. Transparent (96-well plates) and black microplates (OptiPlate-96 well plates) were supplied by Corning Life Sciences and PerkinElmer, respectively. Cell culture flasks (Nunc™ EasYFlask™), fetal bovine serum (FBS), and live/dead calcein AM/ethidium homodimer were obtained from Thermo Scientific. Trypsin, Dulbecco's modified Eagle's medium (DMEM), and C2C12 cells (mouse muscle cells) were supplied by American Type Culture Collection (ATCC, USA). Dulbecco's phosphate-buffered saline (DPBS; no calcium or magnesium) was obtained from Gibco™.

2.2 Film preparation

Clevios PH1000, EG, and TA (chemical structures in Fig. 1(a)) were mixed at the ratios listed in Table 1 in a planetary mixer (ARM-310, Thinky) at 2000 rpm for 10 min. The samples were named according to the description in Table 1. The films were obtained by casting the mixture into a glass mold (with a thickness of ~1 mm) and drying at 60 °C for 90 min. A glass mold coated with transparent scotch tape (3M) was used for preparing PEDOT/EG/TA-3 samples to facilitate de-molding process. The heating temperature and duration was optimized to prevent the formation of bubbles during drying and ensure easy de-molding of PEDOT/EG/TA-3 films. The film thickness was measured using a Mach-1 V500cst MA009 mechanical tester (Biomomentum Inc., Canada) with a spherical stainless-steel indenter with a diameter of 1 mm (values reported in

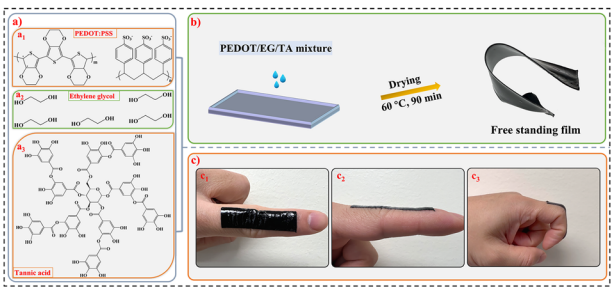

Fig. 1 (a) Chemical structures of PEDOT:PSS (a_1), EG (a_2), and TA (a_3). Schematic of the film preparation (b). Digital pictures of free-standing PEDOT/EG/TA-3 films on finger skin: top view (c_1), side view (c_2), and side view during finger bending (c_3).

Table 1 PEDOT/EG/TA film samples used in this study

Samples	PEDOT:PSS suspension (wt%)	EG (liquid) (wt%)	TA (solid) (wt%)
PEDOT/EG/TA-0	91.0	9.0	0
PEDOT/EG/TA-1	87.5	9.0	3.5
PEDOT/EG/TA-2	84.5	8.5	7.0
PEDOT/EG/TA-3	82.0	8.0	10.0

Table 2 Thickness, tensile Young's modulus in the 0–10% strain range, elongation at break, 90° peeling-off adhesion on glass and porcine skin, and conductivity of the films. The thicknesses ranged between ~65 μm and ~130 μm, depending on the amount of TA. Data for the adhesion force (n = 3), tensile Young's modulus (n = 3), elongation at break (n = 3), and conductivity (n = 5) are reported as mean ± standard deviation

Samples	Thickness (μm)	Young's modulus (kPa)	Elongation at break (%)	Adhesion (N cm^{-1})		Conductivity (S cm^{-1})
				Glass	Porcine skin	
PEDOT/EG/TA-0	~65	1360 ± 123	52.6 ± 1.8	~0.004	~0.004	91.7 ± 4.4
PEDOT/EG/TA-1	~85	1092 ± 54	62.3 ± 4.3	~0.01	0.009 ± 0.002	39.2 ± 2.6
PEDOT/EG/TA-2	~110	513 ± 64	81.3 ± 2.8	4.3 ± 0.8	0.059 ± 0.007	22.0 ± 1.7
PEDOT/EG/TA-3	~130	449 ± 23	90.1 ± 5.4	5.9 ± 0.2	0.700 ± 0.040	16.5 ± 0.7

Table 2). The TA concentration in the mixture was varied to optimize the mechanical properties of the films. The optimal TA concentration was determined by a trade-off between de-molding condition, adhesion, self-healing, and conductivity. For instance, the films cannot be peeled from the mold without damage when the amount of TA is over 10 wt% and they could not provide sufficient adhesion on the skin at low TA contents (*e.g.* <7 wt%). PEDOT/EG/TA-3 films were used for creep deformation, self-healing, and fabrication of epidermal electrodes because of their high stretchability and adhesion properties.

2.3 Electrical conductivity measurement

The electrical conductivity of the samples was measured using a Biomomentum 4-point probe system (Fig. S1, ESI†) connected to a source measure unit (B2902A, Agilent). The current voltage characteristics were acquired with voltage steps of 0.1 V from 0.5 to 1 V. The conductivity (σ) of the films was calculated as follows:

$$\sigma = \frac{L}{R_A \times S} \quad (1)$$

where R_A is the average resistance and L and S are the length and section of the films, respectively. The reported conductivity values represent the average of five measured samples, with the error corresponding to the standard deviation.

2.4 Mechanical characterization

Electromechanical, creep-recovery, and adhesion measurements were performed using a Mach-1 V500cst MA009 mechanical tester (Biomomentum Inc., Canada).

For the electromechanical tests, the end sides of the films (10 mm × 40 mm) were connected to two electrical tensile grips with a gap of 10 mm. The films were stretched at a speed of 6 mm min^{-1} using a 70 N load cell. The tensile rate was set according to the American Society for Testing and Materials (ASTM) 882-10 standard. The resistance ratio was calculated as R/R_0, where R and R_0 are the resistances at a given strain and 0% strain, respectively. The Young's modulus of the films was extracted from the slope of the stress–strain curves in the range of 0–10% strain. Three samples of each film type were tested.

Creep-recovery measurements were performed to evaluate the deformation and recovery behaviors of the films over time. A constant creep stress of 150 kPa was applied to the samples for 5 min, followed by a release for 10 min. The change in strain was measured over time, and the strain recovery was calculated as:

$$\text{Strain recovery } (\%) = \frac{L_0 - L}{L_0} \times 100 \quad (2)$$

where L and L_0 are the lengths of the film during recovery and upon immediate removal of constant stress, respectively.

Adhesion measurements were performed on glass and porcine skin in 90° peeling-off geometry (Fig. S2, ESI†), according to ASTM D6862. The films were treated at 80 °C for 2 min before the test to remove surface moisture. Rectangular pieces of the films (10 mm × 60 mm) were attached to a PET sheet for ease of handling and subsequently transferred to glass or porcine skin (contact area of 10 × 40 mm^2). Adhesion force measurements were performed while detaching the films from the substrate at a speed of 60 mm min^{-1}. Three samples of each film were measured, and the adhesion force was calculated as the average stable force normalized to the width of the film.

2.5 Fourier-transform infrared (FT-IR) spectroscopy

A PerkinElmer Spectrum 65 spectrophotometer was used to record Fourier-transform infrared (FT-IR) spectra in absorption mode, with a scan range of 500–4000 cm^{-1} and 16 scans at a resolution of 4 cm^{-1}.

The spectra of the films (Fig. S3, ESI†) showed the characteristic peaks of TA, EG, and PEDOT:PSS. The broad peak at 3000–3700 cm^{-1} observed for all samples is attributed to the stretching vibration of the –OH groups of EG and TA. The peaks at ~1620 cm^{-1} and ~1380 cm^{-1}, corresponding to the C=C and C–C bonds of the thiophene ring,[26] and the band at ~ 1120 cm^{-1}, corresponding to the –SO_3H group of PSS,[26] indicate the presence of PEDOT:PSS. The peaks corresponding to C–H stretching (at ~2938 cm^{-1} and ~2875 cm^{-1}), C–O stretching (at 1084 cm^{-1}), and C–C–O symmetric stretching (882 cm^{-1}) confirmed the presence of EG.[27] The peak at ~1452 cm^{-1} corresponds to the stretching vibrations of the-C–$C_{aromatic}$ groups in TA.[28]

2.6 Self-healing

The autonomous and cut-stick healing properties of the PEDOT/EG/TA-3 films were evaluated in two different experiments. Three samples of each film type were tested.

2.6.1 Autonomous self-healing. Films (40 mm × 10 mm × 0.13 mm) were placed on a glass slide with both ends connected to two strips of copper tape (40 mm × 5 mm). The current flowing in the film upon application of a 0.02 V bias

was measured with a Keysight source-measure unit (SMU B2902A). A stainless-steel double-edge blade (Feather, Japan) was used to cut the film (the cut width was between 5 and 20 μm) while continuously monitoring the current. An inverted optical microscope (Carl Zeiss, Primovert, Germany) was used to visualize the process in real-time. The mechanical properties after autonomous healing could not be evaluated due to high adhesion of the films on the glass.

2.6.2 Cut-stick self-healing. For electrical healing, two pieces of conductive copper tape were placed at the extremities of two films (contact length of approximately 5 mm), and a light-emitting diode (LED) was connected to the other side of the copper tape. The other extremities of the films were connected with copper tape to an electrical probe station equipped with an Agilent source-measure unit. To observe the electrical healing behavior, the films were cut with a stainless-steel knife blade (Craft Cutter) and successively manually stuck together. A voltage of 3.2 V was applied during the experiment, based on the recommended operating voltage provided in the specification sheet of the LED. The electrical-healing efficiency was calculated as follows:

$$\eta = \frac{I_{\text{healed}} - I_{\text{damaged}}}{I_{\text{pristine}} - I_{\text{damaged}}} \times 100\%, \quad (3)$$

where I is the current measured for the healed, damaged, and pristine films.

For mechanical healing, the films (10 mm × 40 mm) were cut into two parts that were successively manually stuck together (overlap area: 10 mm × 3 mm). Force–displacement tests performed on healed samples were compared with those of the pristine ones. The films were stretched at a speed of 6 mm min^{-1} using a 70 N load cell.

2.7 Preparation of electrodes

The epidermal electrodes were prepared as follows: (i) electrical contacts were made by casting stretchable silver ink onto a PET sheet and drying at 100 °C for 5 min; (ii) PEDOT/EG/TA-3 disks were attached to the silver surface; and (iii) a snap button was attached to the end of the PET sheet for connection to the electronics (Fig. S4, ESI†).

2.8 Characterization of epidermal electrodes

Skin electrode impedance and ECG and EMG measurements were performed as previously described.[29] For EMG recording, positive and negative electrodes were attached to the flexor carpi muscle of the right forearm and a ground electrode was placed on the elbow. Twelve signal regions and 13 noise regions were chosen for the root-mean-square (RMS) signal and RMS noise value calculations, respectively. The protocol for human experiments was approved by the ethical committee of Polytechnique Montreal (approval number CER-2021-04-D). Informed consent was obtained for the experiments involving human participants.

2.9 Biocompatibility assay

Cell culture was performed according to the standards of the American Type Culture Collection (ATCC). C2C12 cells were cultured in a flask in a culture medium containing DMEM with 10% FBS in an incubator (Sanyo MCO-17A, Japan) at a constant temperature of 37 °C in a saturated humidity atmosphere (95% air/5% CO_2). 10 μL sterilized PEDOT:PSS/EG/TA-3 mixture was coated onto the polystyrene (PS) wells, followed by drying at 60 °C overnight. Before cell plating, the coated wells were thoroughly rinsed with DPBS to remove excess acidic residues from the films. The cells were seeded onto PEDOT/EG/TA-3 film-coated PS wells. Uncoated PS wells sterilized with IPA were used as negative controls, whereas untreated wells were used as positive controls. For cell viability studies, 20 000 cells per well were seeded and cultured for 24 h (day-1) and 72 h (day-3). Before the test, the samples were rinsed with DPBS (80 μL) after removing the culture medium on day-1 and day-3. A live/dead calcein AM/ethidium homodimer assay was used to stain the cells according to the manufacturer instruction on day-1 and day-3. Briefly, after rinsing the samples, 80 μL dye solution (4 μM EthD-1 and 2 μM calcein in DPBS) was added and incubated at 37 °C for 30 min before the tests. The cells were observed under a microscope (EVOS M5000, Thermo Scientific, USA). For quantitative viability of cells, black microplates were used for spectrophotometric measurements on a microplate reader (Infinite 200 Pro, Tecan, Switzerland). The fluorescence of the solutions was measured spectrophotometrically at 494 nm excitation and 517 nm emission wavelengths. The cell viability (% live cell) was calculated as follows:

$$\%\ \text{live cell} = \frac{F(517)_{\text{sam}} - F(517)_{\text{min}}}{F(517)_{\text{max}} - F(517)_{\text{min}}} \quad (4)$$

where $F(517)_{\text{sam}}$, $F(517)_{\text{max}}$, and $F(517)_{\text{min}}$ are the average (three samples) fluorescence of PEDOT/EG/TA film-coated wells, positive control wells, and negative control wells, respectively. The reported values of cell viability corresponded to the calculated average value and the error of the standard deviation.

3. Results and discussion

3.1 Film deposition

The films were processed from aqueous mixtures of PEDOT:PSS, EG, and TA (chemical structures in Fig. 1(a)). Free-standing films were obtained by casting the suspensions into molds and heating at moderate temperature (Fig. 1(b)). EG is a well-established conductivity enhancer for PEDOT:PSS, while TA was added to enhance the adhesion properties of the films.[18] With the aim to find the right balance of mechanical and electrical properties, we processed films containing different amounts of TA. Based on the weight percentage of TA, the films were named PEDOT/EG/TA-0 (0 wt% TA), PEDOT/EG/TA-1 (3.5 wt% TA), PEDOT/EG/TA-2 (7 wt% TA), or PEDOT/EG/TA-3 (10 wt% TA).

The PEDOT/EG/TA-3 films in particular, exhibited outstanding mechanical properties. They could be reversibly folded (Fig. 1(b)

and Fig. S5a, ESI†) and exhibited excellent adhesion to the skin and the ability to adapt to rapid finger movements (Fig. 1(c_1)–(c_3) and Movie S1, ESI†), indicating fast response of the films to rapid deformation. Moreover, they could adhere to various materials, such as stainless steel (Fig. S5b, ESI†), copper (Fig. S5c, ESI†), glass (Fig. S5d, ESI†), and PET (Fig. S5e, ESI†) and withstood suspended weights up to 500 g (Fig. S5f and Movie S2, ESI†).

3.2 Mechanical and electrical tensile properties

The electrical conductivities of the films (Table 2) ranged between ~90 S cm^{-1} (PEDOT/EG/TA-0) and ~17 S cm^{-1} (PEDOT/EG/TA-3) and decreased with increasing TA content.

The mechanical properties of the films were assessed by stress–strain measurements (Fig. 2(a)), which showed that increasing the amount of TA led to a decrease of the Young's modulus and an increase of the elongation at break (Fig. 2(b) and Table 2), thus yielding more stretchable films. Electrical resistance measurements, acquired during stress–strain, revealed a very good electrical stability under strain (Fig. 2(c) and Table S1, ESI†). For instance, at 30% strain, the typical human skin stretchability,[15] PEDOT/EG/TA-3 films showed an increase in resistance of only ~2%, which is lower than the values reported in the literature (Table 3).[1,15,18,25] Remarkably, at 90% strain, the increase in resistance was only ~23% of the initial value. These results are promising for applications in epidermal electronics.

To study the effect of TA on the deformation and recovery behavior, we performed a comparative creep recovery test in the presence and absence of TA (PEDOT/EG/TA-3 and PEDOT/EG/TA-0 films, Fig. 2(d). Upon application of constant stress, both films exhibited instantaneous deformation, which steadily increased over time. After five minutes, strain changes of ~10% and ~2.5% were observed for PEDOT/EG/TA-3 and PEDOT/EG/TA-0 films, respectively. Ten minutes after the removal of the stress, the recovery was ~80% for the PEDOT/EG/TA-3 films and ~95% for the PEDOT/EG/TA-0 films (Fig. 2(e)), indicating that the films containing TA had a more pronounced tendency to deform.

The effect of TA on the mechanical properties of the films can be explained by the formation of hydrogen bonds between the hydroxyl groups of TA and EG and the sulfonate groups of PSS and π–π stacking between the hydrophobic benzene groups of TA and PEDOT.[18] These effects likely weaken the electrostatic interaction between PEDOT and PSS chains, thus increasing the polymer chain mobility, which in turn results in enhanced softness and deformation.

3.3 Adhesion properties of PEDOT/EG/TA films

The adhesion properties of the films were studied on glass and porcine skin. The measurements (Fig. 3, data in Table 2) clearly show that the adhesion force increases with the TA content. For a TA content of 10 wt% (PEDOT/EG/TA-3 film), the maximum adhesive force of the films approached 6 N cm^{-1} on glass and 0.7 N cm^{-1} on porcine skin. These values compare well with those of PEDOT:PSS/WPU/D-sorbitol films (*e.g.*, 1.5 N cm^{-1} on the glass and ~0.3 N cm^{-1} on porcine skin)[15] and PEDOT:PSS/PVA/TA films (*e.g.*, ~0.3 N cm^{-1} on the glass and ~0.3 N cm^{-1} on porcine skin).[18] This high adhesion force is likely due to the catechol and pyrogallol aromatic ring structures present in TA, which can form hydrogen bonds with the functional groups of the substrates.[16,17]

3.4 Electrical and mechanical self-healing

Self-healing properties are highly desired to increase the lifetime of epidermal devices, where damages caused by mechanical stress or scratching are inevitable. Our group has reported

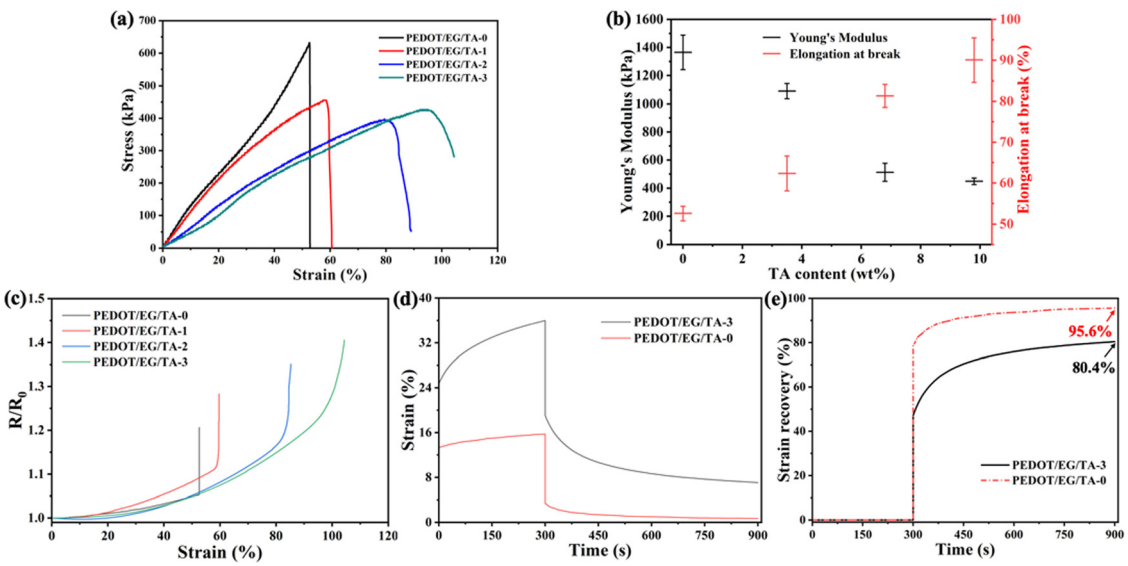

Fig. 2 Mechanical and electrical properties of PEDOT/EG/TA films. (a) Tensile stress *versus* strain. (b) Average tensile Young's modulus at 10% strain and elongation at break of films with different TA content. (c) Electrical resistance *versus* tensile strain of PEDOT/EG/TA films obtained during the stress–strain measurements in Fig. 2(a). (d) Creep deformation (strain *vs.* time) and (e) strain recovery time plots of the PEDOT/EG/TA-0 and PEDOT/EG/TA-3 films. A constant creep stress of 150 kPa was applied for 5 min, and the strain was allowed to recover for 10 min after removing the stress. The tensile Young's modulus (n = 3) and elongation at break (n = 3) of the films are reported as mean ± standard deviation.

Table 3 Comparison of properties of PEDOT-based materials for epidermal electronics

Entry	Form	Components	Young's Modulus	Elongation at break	Adhesion	Conductivity (S cm^{-1})	Electrical stability ($\Delta R/R_0$)	Self-healing	Applications	Ref.
1	Film	PEDOT:PSS, EG, TA	~450 kPa	~90%	~0.7 N cm^{-1} on dry porcine skin	17–90	2% at 30% strain 23% at 90% strain	Autonomous and cut-stick	ECG, EMG	This Work
2	Film	PEDOT:PSS, EG, PVA, TA	~18 MPa	~50%	~0.3 N cm^{-1} on dry skin	~120	15% at 30% strain	N/A	ECG, EMG	18
3	Film	PEDOT:PSS, waterborne polyurethane, D-sorbitol	~40 MPa for 19 wt% PEDOT:PSS	~40% for 38 wt% D-sorbitol	~0.4 N cm^{-1} on dry skin	72–545	~10% at 30% strain	N/A	ECG, EMG, EEG	15
4	Film	PEDOT:PSS, β-cyclodextrin, citric acid, PVA, glutaraldehyde	~56–400 kPa	700%	~1.2 MPa on a polyimide substrate (Lap shear test)	1–37	~10% at 30% strain	N/A	EMG	1
5	Film	PEDOT:PSS, glycerol, polysorbate	~0.8 MPa	~90%	~0.01 N cm^{-1} on porcine skin	70–140	~70% at 90% strain	N/A	EMG	25
6	Film	PEDOT:PSS, poly(2-acrylamido-2-methyl-1-propanesulfonic acid	~0.8 MPa	630%	N/A	320	~25% at 60% strain	Autonomous and mechanical	Pressure sensor, OECT	11
7	Film	PEDOT:PSS, Polyurethane diol	~15 MPa	~30%	~0.07 N cm^{-1} on the glass	~30	~20% at 30% strain	Autonomous	ECG, EMG	30
8	Organohydrogel	PEDOT:PSS, EG, TA	~20 kPa (compressive)	N/A	N/A	~6	N/A	N/A	ECG, EMG	9
9	Hydrogel	PEDOT:PSS, PVA, sulfosuccinic acid	~0.2 kPa	>600%	N/A	~0.02	~10% at 30% strain	Mechanical	Strain sensor	31
10	Hydrogel	PEDOT:PSS, PVA, borax	~4 kPa (compressive)	>10 000%	1.9 N cm^{-12} on porcine skin (perpendicular adhesion)	~5.0×10^{-5}	N/A	Autonomous and cut-stick	ECG, EMG	29
11	Ionogel	PEDOT:PSS, polyaniline, ionic liquids	N/A	N/A	N/A	1250	N/A	N/A	Actuator	32
12	Ionogel	PVA, TA, ionic liquids, PEDOT:PSS, divinyl sulfone	14–70 kPa	N/A	N/A	~0.02 (ionic conductivity)	N/A	N/A	Pressure sensors, ECG	33

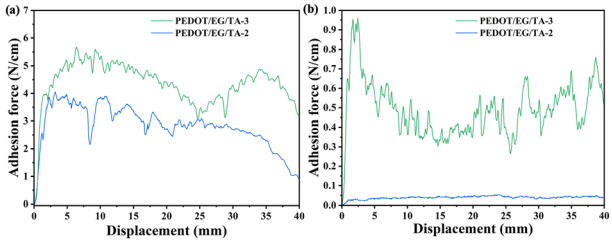

Fig. 3 Adhesion force *versus* displacement for PEDOT/EG/TA-2 (7 wt% TA) and PEDOT/EG/TA-3 (10 wt% TA) films on glass (a) and porcine skin (b). A 90° peeling-off geometry is used. The fluctuations during the peeling process were likely caused by high adhesion on the glass, which led to damage during peeling (Fig. S6, ESI†). The adhesion force decreased to approximately zero for TA contents below 3.5 wt% (Fig. S7, ESI†).

several materials based on PEDOT:PSS, which could achieve water-induced, autonomous or cut-stick healing.[10,12,13] However, a material which can heal both autonomously and via a cut-stick process, with a complete recovery of both electrical and mechanical properties has not been reported so far. The films presented in this work look very promising for achieving these results, based on their softness and adhesion properties imparted by TA. We therefore investigated the effect of the amount of TA on the autonomous and cut-stick healing properties of the films.

Autonomous self-healing properties were studied by measuring the current flowing through the film while cutting it with a sharp blade. The current *versus* time plots of the different samples show that the healing performance improved upon increasing of the TA content (Fig. S8a–c and Movie S3, ESI†), while no self-healing was observed in absence of TA (Fig. S8d and Movie S4, ESI†). PEDOT/EG/TA-3 films (10 wt% TA, Fig. 4(a)) show autonomous recovery of the current to its initial value within approximately 30 s after cut, and repeated healing was observed for multiple damages in different regions of the film (result for an additional sample is shown in Fig. S8a, ESI†). Optical microscope images taken during the process (Fig. 4(b)–(d)) show that the gap created by the cut healed completely within approximately 45 s. Similarly, a real-time video of the process (Movie S3, ESI†) revealed that the healing started immediately after the cut and was completed after approximately 45 s. Interestingly, the self-healing properties were maintained after storage in a fridge at 4 °C for 21 days (Fig. S9, ESI†).

To assess the mechanical healing of the films, we measured their tensile properties after cutting them into two pieces and manually rejoining them. This is referred to as the "cut-stick healing" behavior in this work. The various PEDOT/EG/TA films exhibited different tensile behaviors after the cut-stick healing tests. As in the case of autonomous healing, the performance improved with increasing TA content, with PEDOT/EG/TA-3 films showing the best characteristics. To conduct a comprehensive analysis of the mechanical properties of the sample after cut-stick healing cycle, we determined the stress values by accounting for the thickness difference for the non-overlapped and overlapped area. Healed PEDOT/EG/TA-3 films showed a tensile behavior similar to that of the intact ones (Fig. 5(a) and Fig. S10a, ESI†). They exhibited good cycling stability, able to withstand loading–unloading for 100 cycles at a ramp strain of 30% (Fig. 5(b)). Interestingly, the overlapping parts of the two reconnected films remained intact during the stretching process, while fractures were observed outside of this area (Fig. 5(c)–(e), and Movie S5, ESI†), indicating a rather strong self-adhesion. Moreover, the overlap area experienced reduced stress due to increased thickness (Fig. S11, ESI†). In contrast, for the healed PEDOT/EG/TA-2 films, after stretching for ~15% strain we observed a decreased tensile stress (Fig. S10b, ESI†) and detachment at the overlap region. The PEDOT/EG/TA-1 film showed no cut-stick mechanical healing effect (Fig. S10c, ESI†).

To evaluate the electrical performance after cut-stick healing, we recorded the current flowing into a series circuit, consisting of two PEDOT/EG/TA-3 films connected to an LED, while performing the healing tests on the films. The current was interrupted after the cut and recovered when the two extremities of the cut were stuck together. This process was repeated several times at different locations on the film, and an electrical healing efficiency of approximately 100% was observed for all cut-stick healing cycles (Fig. 6(a)). The LED lit when the circuit was closed (Fig. 6(b)), it turned off when the circuit was opened by cutting one of the films (Fig. 6(c)), and the lit again when the two parts of the film were re-attached (Fig. 6(d) and Movie S6, ESI†).

Overall, PEDOT/EG/TA-3 (10 wt% TA) films demonstrated efficiencies of 100% for both autonomous and cut-stick self-healing. Although further investigation is necessary to clarify the healing mechanism, these remarkable healing properties can be attributed to the mechanical softness and adhesive properties imparted by the presence of TA and the formation of hydrogen bonds between the species present in the films at the gap interfaces (Fig. S12, ESI†). The similar autonomous healing effect was observed in PEDOT:PSS/PEG films.[12] For cut-stick healing,

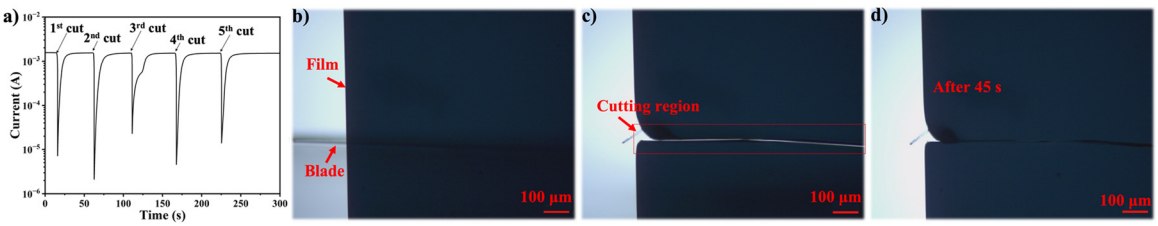

Fig. 4 Electrical and mechanical autonomous healing properties of PEDOT/EG/TA-3 films. (a) Autonomous electrical healing process: current *versus* time measurements were performed under a constant voltage of 0.02 V upon various cutting-healing cycles. Images showing the healing effect of the PEDOT/EG/TA-3 film (b)–(d). Optical microscope images of self-healing process (b) before cutting, (c) after cutting, and (d) after healing.

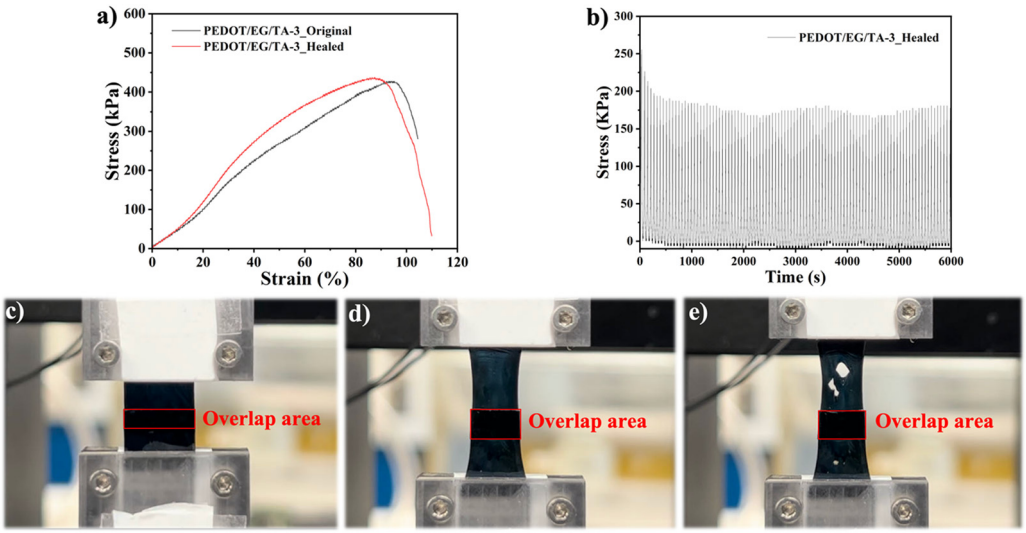

Fig. 5 Mechanical cut-stick healing process of PEDOT/EG/TA-3 films. (a) Tensile stress–strain plots of original and cut-stick healing of films and (b) stretching stability of the healed PEDOT/EG/TA-3 film at a strain of 30%. Stress *versus* time plots for 100 cycles. The stress was calculated based on the thickness of the non-overlap area. Photographs of the healed PEDOT/EG/TA-3 film mounted on the tensile tester (c) before stretching (the overlap area of the film was 10 mm × 3 mm), (d) during stretching, and (e) after appearance of the first fractures.

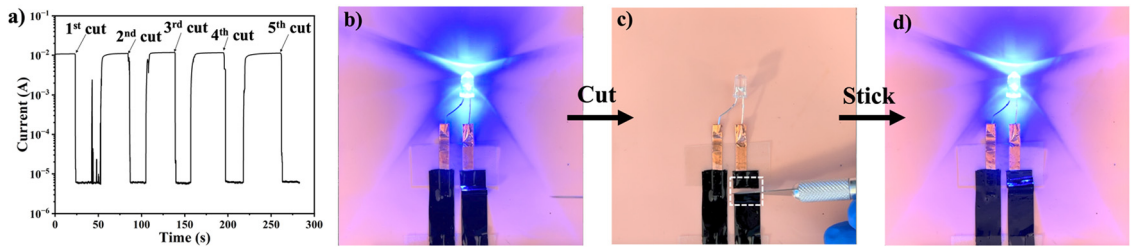

Fig. 6 Electrical cut-stick healing process of PEDOT/EG/TA-3 films: (a) current *versus* time measurements under a constant voltage of 3.2 V after repeated cut-stick healing cycles; (b)–(d) visualization of the healing effect with an LED indicator: (b) original (closed), (c) cut (open), and (d) healed (closed).

the large number of –OH groups in the catechol and pyrogallol aromatic rings of TA play an important role in enhancing healing effectiveness (Fig. S12, ESI†). These –OH groups can lead to high self-adhesion between the two films through the formation of hydrogen bonds. As a result, the two separated films can adhere tightly and self-heal.

The electrical, mechanical, adhesion, and self-healing properties of the PEDOT/EG/TA films and some recently reported PEDOT:PSS-based materials are summarized in Table 3. Our PEDOT/EG/TA films showed low Young's modulus and high adhesion compared to most reported PEDOT:PSS-based films (Table 3). Also, they exhibited a small resistance change ($\Delta R/R_0$) under strain compared to most PEDOT-based materials (Table 3). Besides showing self-healing properties, the PEDOT/EG/TA films here reported feature a good balance of electrical and mechanical properties, although higher value of conductivity and stretchability have been reported. Hence, by mixing TA and EG with PEDOT:PSS, we obtained self-healing films with high adhesion and favorable mechanical and electrical properties for the development of epidermal electrodes.

3.5 Skin-electrode impedance and ECG & EMG recording properties

The outstanding mechanical, electrical, adhesion, and self-healing properties of PEDOT/EG/TA-3 films make them suitable for soft epidermal electronics, which should ideally have a Young's modulus similar to that of the skin and adhere conformally to the skin to ensure the acquisition of high-quality signals.

To evaluate the PEDOT/EG/TA-3 film electrodes, skin electrode impedance *versus* frequency measurements were performed using a three-electrode setup (Fig. S13a, ESI†). We performed the measurements on the same volunteer, location, and during the same day, as the testing conditions (*e.g.*, object, skin conditions, location, and time) can significantly affect the results. In the relevant frequency range up to 100 Hz (Fig. S13b and Table S2, ESI†), the electrodes performed slightly better than the commercial adhesive Ag/AgCl gel disk electrodes (*e.g.*, ~160 kΩ and ~220 kΩ for the film and gel disk electrodes at 10 Hz, respectively; Table S2, ESI†), while they performed similarly at high frequencies.

Monitoring vital signs such as ECG and EMG is critical for point-of-care diagnostics. The ECG biopotentials were recorded by attaching the ground and positive electrodes to the left forearm and the negative electrode to the right forearm (Fig. 7(a)). The ECG voltage *vs.* time plots indicated that the PEDOT/EG/TA film electrodes exhibited well-defined ECG characteristic peaks, including P waves, QRS complexes, and T waves (Fig. 7(b)). In addition, the electrodes demonstrated high ECG recording stability for over 90 seconds (Fig. S14, ESI†). Their performances were similar to those of three different types of commercial Ag/AgCl gel electrodes (Fig. S15a–c, ESI†).

To assess the EMG monitoring ability of the electrodes, we attached positive and negative electrodes to the right forearm and the ground electrode to the elbow of a volunteer (Fig. 7(c)) and recorded the changes in biopotential resulting from switching between relaxed and tense states of the flexor carpi muscle for over 90 seconds. EMG voltage *vs.* time plots showed that the PEDOT/EG/TA film electrodes and three commercial Ag/AgCl gel electrodes showed similar potential changes when switching the state of the muscle (Fig. 7(d) and Fig. S15d–f, ESI†). Notably, the SNR of EMG signals recorded using the PEDOT/EG/TA film electrodes (37.0 ± 1.7 dB) was similar to that achieved using the commercial Natus® (34.1 ± 0.9 dB), 3M® (38.7 ± 0.8 dB), and Ambu® (36.2 ± 0.3 dB) Ag/AgCl gel electrodes (Fig. S15g, ESI†).

The above results indicate that our electrodes are suitable for bio-signal recording. Moreover, they do not require an adhesive tape, owing to the high adhesion of the film electrodes and might benefit from the biocompatibility, antibacterial, antioxidative, and anti-inflammatory properties of TA.[16,17,23]

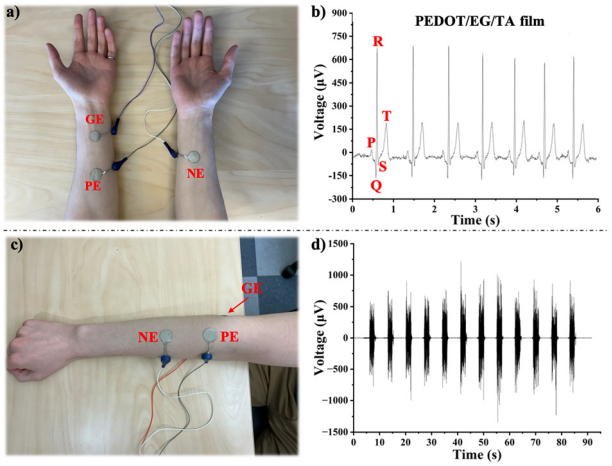

Fig. 7 ECG and EMG signal recordings of PEDOT/EG/TA film electrodes. (a) Configuration of ECG measurements in a volunteer. Positive (PE) and ground (GE) electrodes were placed on the left forearm and the negative electrode (NE) was placed on the right forearm. (b) ECG biopotentials (voltage *versus* time) recorded using PEDOT/EG/TA-3 film electrodes. (c) Configuration of EMG measurements in a volunteer. EMG biopotentials between the electrodes were recorded with PE and NE on the right forearm and GE on the elbow. (d) EMG monitoring using the PEDOT/EG/TA film electrodes.

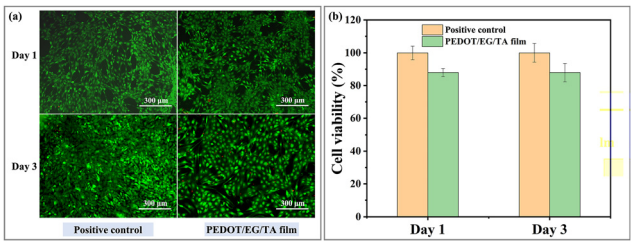

Fig. 8 (a) Representative images of the live/dead assay of mouse muscle cells (C2C12) cultured on uncoated (positive control) and PEDOT/EG/TA-3 film-coated PS substrates for one and three days. (b) Quantitative analysis of cell viability. As a negative control, cell viability was approximately 0. Error bars represent the standard deviation (n = 3).

3.6 Biocompatibility assay

We assessed the cytotoxicity of the PEDOT/EG/TA films by culturing C2C12 muscle cells on their surfaces. Fig. 8(a) shows the staining results of the cells cultured on PEDOT/EG/TA film-coated and uncoated (positive control) wells with live (green) and dead cells (red). As confirmed by the predominance of green coloration (red coloration only visible at high magnification), the cells adhered to and proliferated on the PEDOT/EG/TA film-coated surfaces, with only a slight difference observed between the positive control and PEDOT/EG/TA film samples. Fig. 8(b) shows that the relative cell viability, that is, the cell viability compared to the positive control group, on the PEDOT/EG/TA film was 88%, which was higher than the non-cytotoxicity criterion (70% of the control group) according to ISO 10993-5.[34] In addition, the relative cell viability of the PEDOT/EG/TA film remained stable until day three. These results indicate that the PEDOT/EG/TA film provides a safe environment for cell growth, thereby ensuring its use in biological applications.

4. Conclusions and perspectives

In summary, we demonstrated stretchable, soft, adhesive, and self-healing conducting polymer films processed from an aqueous mixture of PEDOT:PSS, EG, and TA. The addition of TA to the PEDOT:PSS-EG system results in materials with enhanced mechanical properties, high adhesion, and outstanding self-healing behavior. The films exhibited no cytotoxicity and provided a safe environment for cell proliferation. Using PEDOT/EG/TA-3 films, we fabricated epidermal patch electrodes exhibiting low skin-electrode impedance at low frequencies and high-quality ECG and EMG signal recording, similar to commercial Ag/AgCl gel electrodes. Our study provides a facile, straightforward, environment friendly, and effective method for developing stretchable, self-healing, and adhesive conductive materials for soft electronics and bio-applications. We believe that the most important challenges in future soft epidermal electronics are fine-tuning the mechanical properties, conductivity, and adhesion of materials and the integration of the materials into soft patch electrodes, endowing wearable devices with more comfortable, reliable, and suitable properties for a wide range of applications.

Author contributions

Xin Zhou: methodology, performing experiments, data collection and analysis, drawing figures, and manuscript preparation. Pierre Kateb, Jiaxin Fan, and Jinsil Kim: data analysis, reviewed & edited manuscript. Gregory A. Lodygensky: ECG and EMG data analysis and reviewed & edited manuscript. Bénédicte Amilhon: biocompatibility data analysis and reviewed & edited manuscript. Damiano Pasini: mechanical data analysis and reviewed & edited manuscript. Fabio Cicoira: supervision, resources, funding acquisition, project administration, reviewed & edited manuscript.

Conflicts of interest

The authors declare that they have no competing financial interests or personal relationships that could influence the work reported in this study.

Acknowledgements

The authors are grateful to Eric Quenneville (Biomomentum) for fruitful discussions. This research was supported by the Natural Science and Engineering Council Canada (NSERC) through Discovery Grants awarded to FC and DP, by a grant from the Transmedtech Institute (Canada First Research Excellence Fund) awarded to FC and GAL, and National Defence Canada (IDEas project CFPMN1-008, awarded to FC). The equipment and infrastructure used in this study were acquired and maintained by the Canada Foundation for Innovation. XZ is grateful to the China Scholarship Council for a PhD scholarship. JK acknowledges the Trottier Energy Institute for a PhD scholarship. PK acknowledges the Pierre Arbour Foundation and NSERC for a Master's scholarship. JF acknowledges the financial support from the NSERC postdoctoral fellowship.

References

1 P. Tan, H. Wang, F. Xiao, X. Lu, W. Shang, X. Deng, H. Song, Z. Xu, J. Cao, T. Gan, B. Wang and X. Zhou, *Nat. Commun.*, 2022, **13**, 358.
2 A. J. Bandodkar, R. Nunez-Flores, W. Jia and J. Wang, *Adv. Mater.*, 2015, **27**, 3060–3065.
3 T. R. Ray, J. Choi, A. J. Bandodkar, S. Krishnan, P. Gutruf, L. Tian, R. Ghaffari and J. A. Rogers, *Chem. Rev.*, 2019, **119**, 5461–5533.
4 T. Kim, J. Park, J. Sohn, D. Cho and S. Jeon, *ACS Nano*, 2016, **10**, 4770–4778.
5 D. H. Kim, N. Lu, R. Ma, Y. S. Kim, R. H. Kim, S. Wang, J. Wu, S. M. Won, H. Tao, A. Islam, K. J. Yu, T. I. Kim, R. Chowdhury, M. Ying, L. Xu, M. Li, H. J. Chung, H. Keum, M. McCormick, P. Liu, Y. W. Zhang, F. G. Omenetto, Y. Huang, T. Coleman and J. A. Rogers, *Science*, 2011, **333**, 838–843.
6 J. W. Jeong, W. H. Yeo, A. Akhtar, J. J. Norton, Y. J. Kwack, S. Li, S. Y. Jung, Y. Su, W. Lee, J. Xia, H. Cheng, Y. Huang, W. S. Choi, T. Bretl and J. A. Rogers, *Adv. Mater.*, 2013, **25**, 6839–6846.
7 L. V. Kayser and D. J. Lipomi, *Adv. Mater.*, 2019, **31**, 1806133.
8 C. Xie, X. Wang, H. He, Y. Ding and X. Lu, *Adv. Funct. Mater.*, 2020, **30**, 1909954.
9 X. Zhou, P. Kateb, F. Miquet-Westphal, G. A. Lodygensky and F. Cicoira, *Adv. Sensor Res.*, 2023, 202300072.
10 Y. Li, X. Zhou, B. Sarkar, N. Gagnon-Lafrenais and F. Cicoira, *Adv. Mater.*, 2022, **34**, 2108932.
11 X. Su, X. Wu, S. Chen, A. M. Nedumaran, M. Stephen, K. Hou, B. Czarny and W. L. Leong, *Adv. Mater.*, 2022, **34**, 2200682.
12 Y. Li, X. Li, S. Zhang, L. Liu, N. Hamad, S. R. Bobbara, D. Pasini and F. Cicoira, *Adv. Funct. Mater.*, 2020, **30**, 2002853.
13 S. Zhang and F. Cicoira, *Adv. Mater.*, 2017, **29**, 1703098.
14 V. P. Vu, L. H. Sinh and S. H. Choa, *ChemNanoMat*, 2020, **6**, 1522–1538.
15 L. Zhang, K. S. Kumar, H. He, C. J. Cai, X. He, H. Gao, S. Yue, C. Li, R. C. Seet, H. Ren and J. Ouyang, *Nat. Commun.*, 2020, **11**, 4683.
16 C. Chen, H. Yang, X. Yang and Q. Ma, *RSC Adv.*, 2022, **12**, 7689–7711.
17 Z. Guo, W. Xie, J. Lu, X. Guo, J. Xu, W. Xu, Y. Chi, N. Takuya, H. Wu and L. Zhao, *J. Mater. Chem. B*, 2021, **9**, 4098–4110.
18 J. Cao, X. Yang, J. Rao, A. Mitriashkin, X. Fan, R. Chen, H. Cheng, X. Wang, J. Goh, H. L. Leo and J. Ouyang, *ACS Appl. Mater. Interfaces*, 2022, **14**, 39159–39171.
19 H. Fan, L. Wang, X. Feng, Y. Bu, D. Wu and Z. Jin, *Macromolecules*, 2017, **50**, 666–676.
20 C. Chen, X. Yang, S.-J. Li, C. Zhang, Y.-N. Ma, Y.-X. Ma, P. Gao, S.-Z. Gao and X.-J. Huang, *Green Chem.*, 2021, **23**, 1794–1804.
21 X. Gao, Q. Dai, L. Yao, H. Dong, Q. Li and X. Cao, *Biomater. Sci.*, 2020, **8**, 2694–2701.
22 H. Fan, J. Wang and Z. Jin, *Macromolecules*, 2018, **51**, 1696–1705.
23 W. Shi, Y. Kong, Y. Su, M. A. Kuss, X. Jiang, X. Li, J. Xie and B. Duan, *J. Mater. Chem. B*, 2021, **9**, 7182–7195.
24 Z. Yi, Y. Zhao, P. Li, K. Ho, N. Blozowski, G. Walker, S. Jaffer, J. Tjong, M. Sain and Z. Lu, *Appl. Surf. Sci.*, 2018, **448**, 583–588.
25 W. Tang, Y. Zhou, S. Chen, S. Yu, Y. Yang, J. Lin, S. Yin, Y. Ma and B. Hu, *ACS Mater. Lett.*, 2021, **3**, 1385–1393.
26 S. Khasim, A. Pasha, N. Badi, M. Lakshmi and Y. K. Mishra, *RSC Adv.*, 2020, **10**, 10526–10539.
27 H. Çabuk, Y. Yılmaz and E. Yıldız, *Acta Chim. Slov.*, 2019, **66**, 385–394.
28 M. A. Pantoja-Castro and H. González-Rodríguez, *Rev. Latinoam. Quim.*, 2011, **39**, 107–112.
29 X. Zhou, A. Rajeev, A. Subramanian, Y. Li, N. Rossetti, G. Natale, G. A. Lodygensky and F. Cicoira, *Acta Biomater.*, 2022, **139**, 296–306.
30 P. Kateb, J. Fan, J. Kim, X. Zhou, G. A. Lodygensky and F. Cicoira, *Flexible Printed Electron.*, 2023, **8**, 045006.
31 S. Wang, G. Guo, X. Lu, S. Ji, G. Tan and L. Gao, *ACS Appl. Mater. Interfaces*, 2018, **10**, 19133–19142.
32 H. Hu, S. Zhang, Y. Li, X. Hu, L. Xu, A. Feng, G. Cheng and J. Ding, *J. Bionic Eng.*, 2023, **20**, 2755–2763.
33 G. C. Luque, M. L. Picchio, A. P. S. Martins, A. Dominguez-Alfaro, N. Ramos, I. del Agua, B. Marchiori, D. Mecerreyes, R. J. Minari and L. C. Tomé, *Adv. Electron. Mater.*, 2021, **7**, 2100178.
34 Biological Evaluation of Medical Devices – part 5: Tests for *In Vitro* Cytotoxicity. 2009.